

JAAS

Accepted Manuscript



This is an *Accepted Manuscript*, which has been through the Royal Society of Chemistry peer review process and has been accepted for publication.

Accepted Manuscripts are published online shortly after acceptance, before technical editing, formatting and proof reading. Using this free service, authors can make their results available to the community, in citable form, before we publish the edited article. We will replace this *Accepted Manuscript* with the edited and formatted *Advance Article* as soon as it is available.

You can find more information about *Accepted Manuscripts* in the [Information for Authors](#).

Please note that technical editing may introduce minor changes to the text and/or graphics, which may alter content. The journal's standard [Terms & Conditions](#) and the [Ethical guidelines](#) still apply. In no event shall the Royal Society of Chemistry be held responsible for any errors or omissions in this *Accepted Manuscript* or any consequences arising from the use of any information it contains.

ARTICLE

Laser ablation and inductively coupled plasma mass spectrometry focusing on bioimaging from elemental distribution using MatLab software: a practical guide

Cite this: DOI: 10.1039/x0xx00000x

Received 00th January 2012,
Accepted 00th January 2012

DOI: 10.1039/x0xx00000x

www.rsc.org/

Gustavo de S. Pessôa^{a,b}, José L. Capelo-Martínez^{c,d}, Florentino Fdez-Riverola^{e,f}, Hugo López-Fernández^{e,f}, Daniel Glez-Peña^{e,f}, Miguel Reboiro-Jato^{e,f}, and Marco A. Z. Arruda^{*a,b}

The parameters influencing laser ablation inductively coupled plasma mass spectrometry as a tool for elemental imaging distribution in tissues are critically commented in this work, and penile cancer tissue was used as a model. General aspects of LA-ICP-MS are discussed, and among them, issues regarding sample preparation and calibration. The optimization process of the following variables is described in detail in a step-by-step tutorial manner: laser intensity, laser frequency, laser resolution, ICP radiofrequency, nebulizer and auxiliary gas flow rates, and C isotopes as internal standards. Once the best condition is found for each variable, MATLAB software is used to generate two-dimensional images. Herein it is also easily explained how to use the MATLAB software to generate the tissue image using the acquisition, exporting and data treatment parameters.

1. Introduction

The importance of visualizing things is highlighted by the adagio “a picture is worth a thousand words”.¹ The meaning of this popular expression is applied in science as well, because researchers try to capture the complexity of problems in a single image.

Advances in electronics, optics, chemistry and software allow currently obtaining high resolution images of virtually any event. Thus, surgeons can currently monitor the frontier between healthy and cancer tissues with the best precision ever thanks to imaging techniques, allowing an almost perfect resection of the cancer tissue.² Furthermore, spatial distribution within a tissue of molecules, such as drugs or biomarkers, is presently followed through imaging.^{3,4}

The acquisition of molecular- or elemental-based images of tissues, organs or even whole body sections is relatively recent.^{5,6} To obtain such images different mass spectrometry-based techniques are used. Laser ablation inductively coupled plasma mass spectrometry, LA-ICP-MS, is the reference technique for qualitatively and quantitatively imaging the spatial distribution of metals and metalloids in a tissue.^{3,7-10} Briefly, LA-ICP-MS is based on the use of a laser offering sufficient energy to ablate the sample (the use of Nd:YAG based lasers operating at 213 or 266 nm is very popular for this purpose). The laser pulse creates the ablation process, vaporizing the sample, which is transferred through an argon gas (or others) to the ICP torch.

Compared to other imaging techniques LA-ICP-MS is cost-effective and sensitive. Furthermore, it does not require sophisticated software neither a previous intensive training to handling the technique properly. To the best of our knowledge, there is no tutorial addressing how to work with LA-ICP-MS neither how to handle the

enormous amount of data generated. This fact hampers this technique to get spread further among the scientific community. This work is intended to cover this gap explaining step by step all the variables affecting the experimental part as well as how to handle the software needed to generate the images, in order to help not only those experts in LA imaging, but mainly also those new users.

For this task, optimization of the main laser variables will be firstly described, then those ones involving the ICP-MS, and, finally, the acquisition and treatment of data for obtaining the bioimages utilizing the MATLAB program. In this context, phosphorus distribution was taken as example. This element has been evaluated in several types of cancer, since it is involved in post-translational modifications of proteins that are involved in the progress of tumor cells.¹¹ The level of phosphorus increases in patients with lymphoma cell, suggesting that cancerous cells have a highest tendency in accumulating this element in the DNA than the normal cells.^{12, 13}

2. Experimental

2.1. Sample preparation

Some informations were previously described, presenting the clinical and histopathological data, age of patients, sample preparation and storage.³ Briefly, tissues of penile cancer samples were kindly provided by A.C. Camargo Cancer Center and Barretos Cancer Hospital. Patients were submitted to surgery, considering the WHO International Classification of Diseases of Oncology.¹⁴ Fresh frozen tissues were inserted in tissue-Tek OCT compound (Sakura, USA). Afterwards, 30 µm-thick sections were cut in a cryostat (Leica CM1850, Leica Microsystems, Wetzlar, Germany). Finally, samples were stored at -80°C.

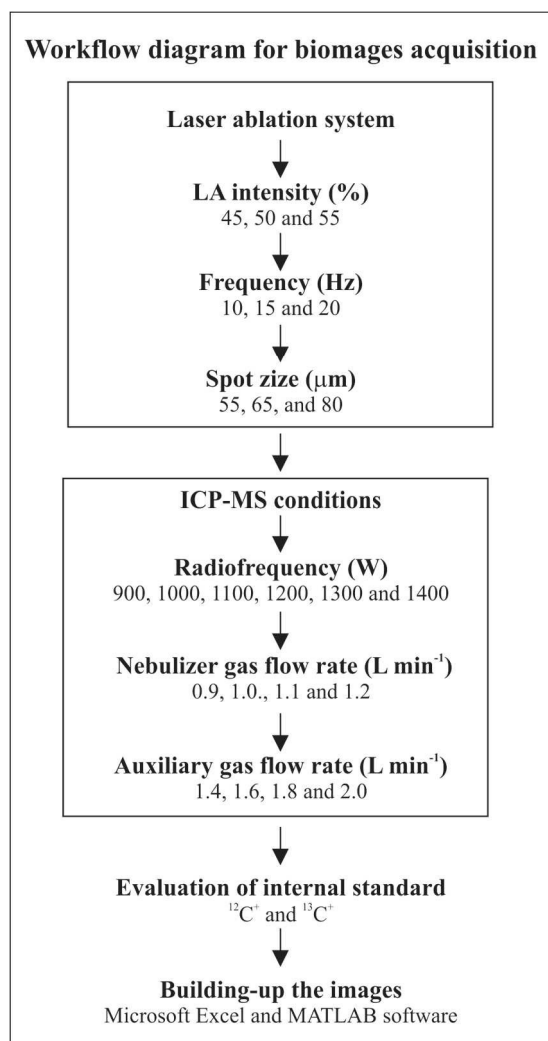


Figure 1. Workflow diagram for optimization purposes.

2.2. Instrumental

LA-ICP-MS analyses were performed in a class 10000 clean room. A LA system (New Wave, UP-213, USA) with a Nd:YAG (213 nm) laser source was used. The parameters affecting LA-ICP-MS performance are shown in Figure 1 along with the corresponding levels assessed in this study.

Laser parameters were adjusted to obtain the best sensitivity and resolution as well as reasonable analysis time, resulting in a complete removal of the material from the tissue. Laser was warmed-up for 5 s. A blank was done so the background signal from the gas was recorded to be subtracted from samples. After each single laser ablation, the chamber was cleaned with argon for 5 s.

The tissue was ablated in multiple parallel lines for building-up maps of elements distribution and for optimizing laser conditions, such as intensity (%) and frequency (Hz). Carbon isotopes were evaluated as internal standard candidates to normalize the mass spectrometry signals and to compensate variations in the ablation process due to sample heterogeneity or to laser intensity variations.

Analyte distributions ($^{12}\text{C}^+$, $^{13}\text{C}^+$, $^{28}\text{Si}^+$ and $^{31}\text{P}^+$) were obtained through a quadrupole-based ICP-MS (PerkinElmer ELAN DRC-e), and the acquisition was carried out after the stabilization of the background signal. A solution of Mg, In, Ba and U was used for the optimization of operational conditions, checking the double charge

Table 1. Optimized instrumental operational conditions and measurement by LA-ICP-MS.

Instrument settings	
Nebulizer	Meinhard
Spray chamber	Cyclonic
RF Power (W)	1300
Nebulizer gas flow (L min⁻¹)	1.0
Auxiliary gas flow (L min⁻¹)	2.0
Data acquisition parameters	
Reading mode	Peak hopping
Detector mode	Pulse
Sweeps	3
Dwell Time (ms)	50
Integration Time (ms)	477 (for each point)
Detector dead time (ns)	60
Lens voltage (V)	Automatic mode
Monitored isotopes	^{12}C , ^{13}C , ^{28}Si and ^{31}P
Laser conditions	
Wavelength of Nd:YAG laser (nm)	213
Laser ablation intensity (%)	50
Frequency (Hz)	20
Spot size (µm)	65
Scan speed (µm s ⁻¹)	60
Resolution – X axis (µm)	28.62
Resolution – Y axis (µm)	80
Average energy output (mJ);	0.036 – 0.045
Average Fluence (J cm ²)	1.10 – 1.35

species and production of oxides were monitored. For all optimization conditions, the measurements were carried out in triplicate.

2.3. Building-up the image

Tissues were ablated line by line with a y-offset distance of 80 µm, using a spot size of 65 µm, and a scan speed of 60 µm s⁻¹.

ICP-MS data obtained after the ablation were exported to the Microsoft Office Excel 2016 (Microsoft Corporation) for all data treatment. The software Matrix Laboratory (MATLAB) version 6.5 was used to built-up the images of the scanned tissues. Main optimized parameters (highlighted in bold) for data acquisition are observed in Table 1.

3. Results and discussion

3.1 General aspects for laser ablation imaging

3.1.1 Sample preparation

In the evaluation of elemental distribution, the use of native sample preparation conditions is desirable since that the image should represent a very close panel of the physiological condition. Thus, the main challenge is to avoid the production of artifacts, which they may arise due to improper drying of the sample, or the use of classical techniques of anatomy and histology. For instance, formalin can leach several metal species, and the use of alcoholic solutions for fixing tissues in paraffin can lead to a reduction up to 40% of the specimen volume.^{15, 16}

In this way, some choices can be made to minimize these problems. For example, the correct type of slide should be chosen for use as support of the histological section, which it should provide the best adhesion of the material and the lowest increase in the

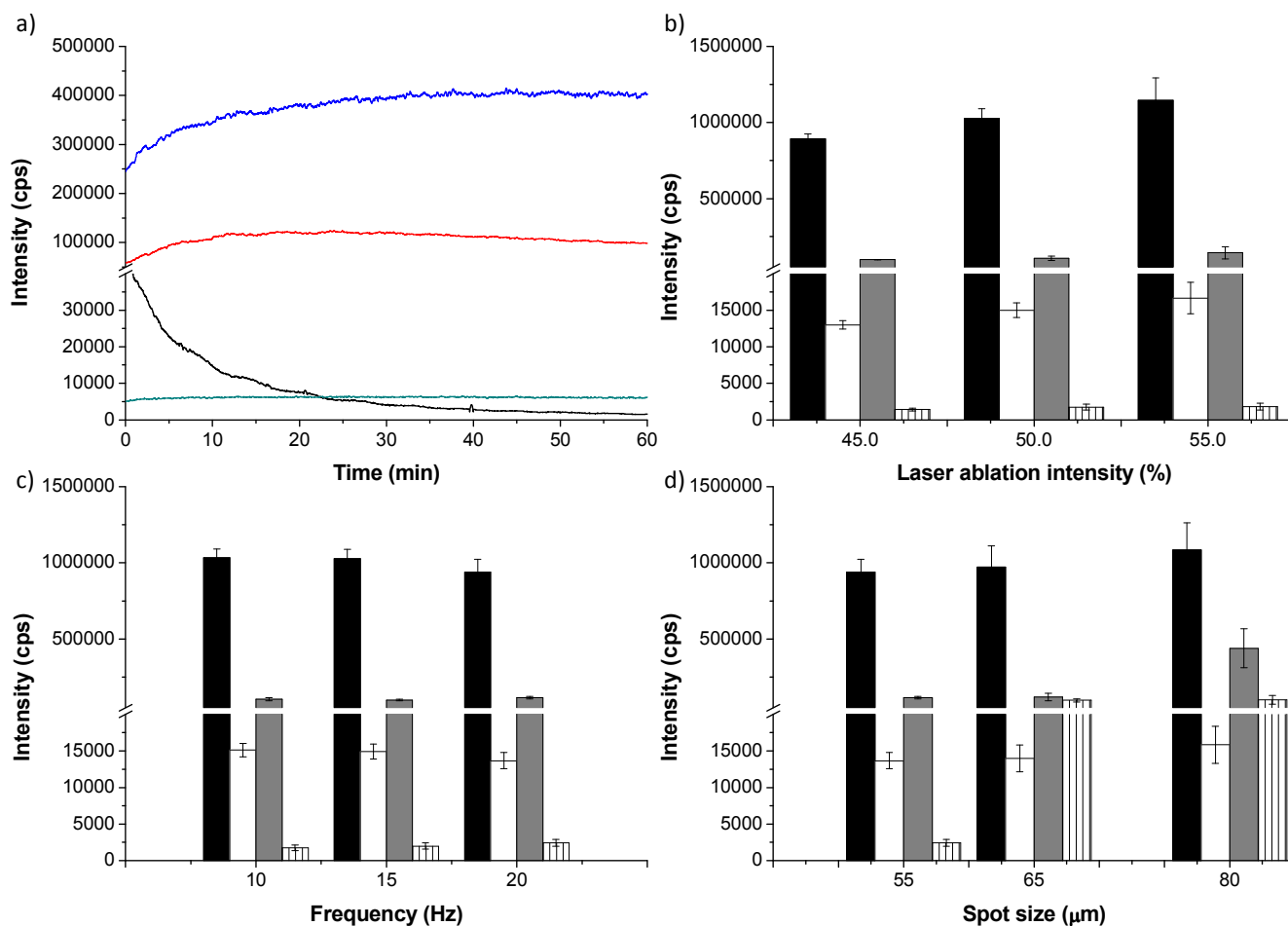


Figure 2 – Optimization of LA system for image acquisition. (a) Background signal for $^{12}\text{C}^+$ (—), $^{28}\text{Si}^+$ (—), $^{31}\text{P}^+$ (—), $^{13}\text{C}^+$ (—). Mass spectrum was smoothed by Savitzky-Golay method, using 2nd polynomial order and 50 points of window. Absolute intensities (cps) for $^{12}\text{C}^+$ (■), $^{13}\text{C}^+$ (□), $^{28}\text{Si}^+$ (■) and $^{31}\text{P}^+$ (□), in relation to (b) laser ablation intensity (%), (c) Frequency (Hz) and (d) Spot size (μm).

background signal. Additionally, the assembly of the histological section and sample drying procedures could be other pitfall in imaging using LA-ICP-MS, and they have been thoroughly presented previously.¹⁷ At this moment, frozen section procedures (native cryosections) seem the ideal sample preparation.

3.1.2 Calibration

In quantitative analysis, the matrix effect is the main pitfall to be overcome. Changes in sample compositions lead to an alteration in the positive charge density of the ion beam, which affects the efficiency of how the ions are guided into the quadrupole. For example, matrix effect can be introduced not only in the site of ablation, but also during the sample transport phase.¹⁸ Then, four strategies are showed: (i) the use of Certified Reference Materials (CRMs); (ii) laboratory prepared standards; (iii) on-line addition; and (iv) isotope dilution.

CRMs provide a sample with known composition for accurate calibration, since they are thoroughly characterized. The analyst can use the CRM to obtain an analytical curve, by the addition of a standard solution. After homogenization, the CRM are pressed at 7 psi, producing pellets with different concentrations of the analytes. In this way, the analyst can compare the results between the quantification using laser ablation, and those ones obtained from a traditional determination, using microwave decomposition and liquid introduction to validate all the procedure.⁹ However, some limitations can be cited, such as, the lack of information regarding the homogeneity in micrometric scale and the absence of suitable standards for quantitative purposes.¹⁹

The most commonly application observed for quantitative analysis using laser ablation is laboratory prepared standards, using the tissue of interest (or analogous), which it is spiked with known amounts of elements of interest. For this task, a tissue is homogenized with pestle and mortar, and, then, mixed with a standard solution, keeping constant the volume of solution. In

1 general, samples with different masses or spiked solutions with
2 different concentrations can be used to prepare the standards, for
3 obtaining the analytical curve. After this step, slices of the standard
4 samples can be obtained from cryo-cutting in a cryostat, or,
5 alternatively, like a pellet. This kind of strategy minimizes the
6 interferences arising from the sample matrix.²⁰ Two aspects are still
7 important to note: (i) the validation of the results by ICP-MS after
8 microwave decomposition is mandatory, in this case, and (ii)
9 standards and samples should be placed together in the ablation
10 chamber.

11 Alternatively, on-line addition of standard solutions have been
12 applied for quantification using LA-ICP-MS. Briefly, a nebulizer is
13 responsible to introduce a standard solution with different
14 concentrations of the analyte. Dressler, et al.,²¹ proposed a
15 quantitative method using a pneumatic nebulization and laser
16 ablation in order to arrange matrix-matching. Ablated material was
17 introduced by laser, while calibration solution was nebulized. Both
18 aerosols were introduced in the injector tube. Several positions for
19 the standard solution nebulizer aerosol have been evaluated in the
20 literature. The current consensus indicates that the nebulizer must be
21 positioned after the ablation chamber, since this geometry reduces
22 problems related to the matrix effect.²² Main limitations of this
23 strategy are the reduced sensitivity and matrix effects, which can
24 occur in conditions of non-equivalent particle size distribution.²³

25 Isotope dilution (ID) has been considered one of the most precise
26 and accurate means for quantification in analytical chemistry.
27 Briefly, ID is based on enrichment of a sample with a standard
28 where one or more isotopes are spiked in a known ratio. Thus, the
29 isotope ratios are measured. Two methods can be used in this
30 approach: pressed pellets or on-line addition. Alternatively, Urgast,
31 et al.,²⁴ injected saline solutions enriched with stable Zn isotopes in
32 animal model for evaluation of the kinetics of essential elements
33 within individual animals at microscale level. Authors found
34 different isotope ratios were identified among the studied organs,
35 such as hippocampus, amygdala, cortex and hypothalamus,
36 suggesting that these regions have differential zinc metabolism
37 kinetics. The main limitation of ID is necessity of two stable
38 isotopes, at least, for carrying out this kind of strategy. However, it
39 is need to emphasizes that LA-ICP-MS is the only technique capable to
40 provide images concerning the isotopic composition of a sample.^{24, 25}

3.2. Evaluation of laser parameters

41 To this section, the optimization of laser parameters will be focused
42 taken into account the laser (Nd:YAG) UP-213 from New Wave.
43 However, an elegant discussion about other lasers equipment can be
44 found in the review of Becker *et al.*¹⁷ Plasma needs to get stabilized
45 over time to obtain reliable results, mainly considering those ones
46 for imaging acquisition. In other words, high or low intensity of
47 different analytes at the beginning of the analysis are not necessarily
48 related to their presences in the sample, but the lack of plasma
49 stabilization time. As an example about the variation in the
50 background signal over time, we observed an increase for the $^{12}\text{C}^+$,
51 $^{13}\text{C}^+$ and $^{28}\text{Si}^+$, signals of about 64.3%, 19.4% and 60.7%,
52 respectively, during one hour of analysis (Fig. 2a).

53 On the other hand, a decrease of *ca.* 29 times was observed for
54 $^{31}\text{P}^+$. Furthermore, other elements such as Fe and Ca can undergo the
55 same behavior. Therefore, as the sample is introduced into the
56 plasma through the sample ablation with the laser, three main
57 variables affecting plasma stability were identified as follows: laser
58 intensity, laser frequency and laser resolution.

59 Laser ablation intensity should be the first parameter evaluated,
60 because it is related to its energy and fluence applied over the
sample. Hence, the laser intensity was varied at 45, 50 or 55%, once
that below 45% intensity not enough material is ablated to signal

acquisition, and over 55%, a certain amount of material from the
sample support is ablated together with the sample material. The
values of energy obtained were 0.012, 0.025, and 0.107 mJ, for 45,
50 or 55%, respectively, while the fluence was ranged from 0.42 and
0.51, from 0.93 and 1.0, and from 4.3 to 4.5 J/cm² for the same
parameters. It is important to notice that such laser intensities are
dependent on the material thickness, needing to optimize in each
case. As can be seen in Figure 2b, an increase in the values for all
elements evaluated was observed when the LA intensity was
increased. When the laser intensity was varied between 45% and
55% the signals for $^{12}\text{C}^+$, $^{13}\text{C}^+$, $^{31}\text{P}^+$, and $^{28}\text{Si}^+$ were increased by
29%, 28%, 22% and 36%, respectively. As P and Si are used to
monitor the ablation over the sample, the intensity for P should be
the highest and the lowest for Si, since they are, respectively, the
analyte and the marker used for monitoring the material removal
from the microscope slide (glass). This compromise is attained at a
laser intensity of 50%. It is worth to mention that the RSDs for the
analytical measurements get highly increased when the laser
intensity was augmented from 45% to 55%. For example the RSD
values for $^{28}\text{Si}^+$ raised from 1% up to 28%. This trend was observed
for other elements. However, at an intensity of 50% RSDs have a
value *ca.* to 6.3, 6.7, 13.0 and 22.4 for $^{12}\text{C}^+$, $^{13}\text{C}^+$, $^{28}\text{Si}^+$ and $^{31}\text{P}^+$,
respectively. This was another reason to choose 50% as the reference
intensity.

Laser frequency refers to the number of times that the laser is
fired against the sample per unit of time (s),²⁷ and this was the
second variable assessed. For this task, the LA intensity, spot size
and scan rate were settled at 50%, 55 μm and 60 $\mu\text{m s}^{-1}$,
respectively. As shown in Figure 2c, three frequency conditions
were tested (10, 15 and 20 Hz) since lower frequencies were
incompatible with the scan rate used. The highest frequency tested
increases the analytical response, for instance a 39% for $^{31}\text{P}^+$. Taking
into consideration that 20 Hz is the maximum frequency that can be
used in such equipment, this level was chosen as the best one.

The spot size is determined by the laser beam diameter (μm) and
it was the third parameter evaluated. It is necessary to stress out that
the spot size must be compatible with the scan speed, in order to
avoid lack of ablation in some spots during the scanning process.²⁵ A
region of 60 μm was programmed to be scanned every second. If the
laser resolution becomes too low or too high, then the performance
becomes far from appropriate. This is because a resolution lowers
than 60 μm will lead to a fail in spatial resolution. As consequence
regions of the tissue will not be ablated. A laser resolution higher
than 60 μm will lead to an excessive ablation in some zones.
Therefore, three conditions were evaluated to assess the influence of
laser resolution: 55 μm , 65 μm and 80 μm . The increase on laser
beam diameter provided the highest analytical signal, as shown in
Figure 2d. This profile was expected, since the amount of ablated
material increases with the laser diameter. The $^{31}\text{P}^+$ signal was
increased a 4000% when the laser resolution was increased from 55
 μm to 65 μm , and a further 4% when it was augmented from 65
 μm to 80 μm . On the other hand, the $^{28}\text{Si}^+$ signal was increased a 1500%
when the laser resolution was varied from 55 μm to 80 μm . As the
method requires maintaining the ratio P-signal to Si-signal as high as
possible the laser resolution was settled in 65 μm .

3.3. Evaluation of ICP-MS parameters

Changes in the composition of the aerosol highly affect the plasma
dynamics, which may be compensated by the radio frequency, RF,
power.²⁸ For this reason RF power was the first parameter to be
evaluated. As shown in Figure 3a, an increase in the signal of all
elements was observed up to 1300 W. It must be stressed out that the
use of high RF power can be necessary for the formation of $^{31}\text{P}^+$,

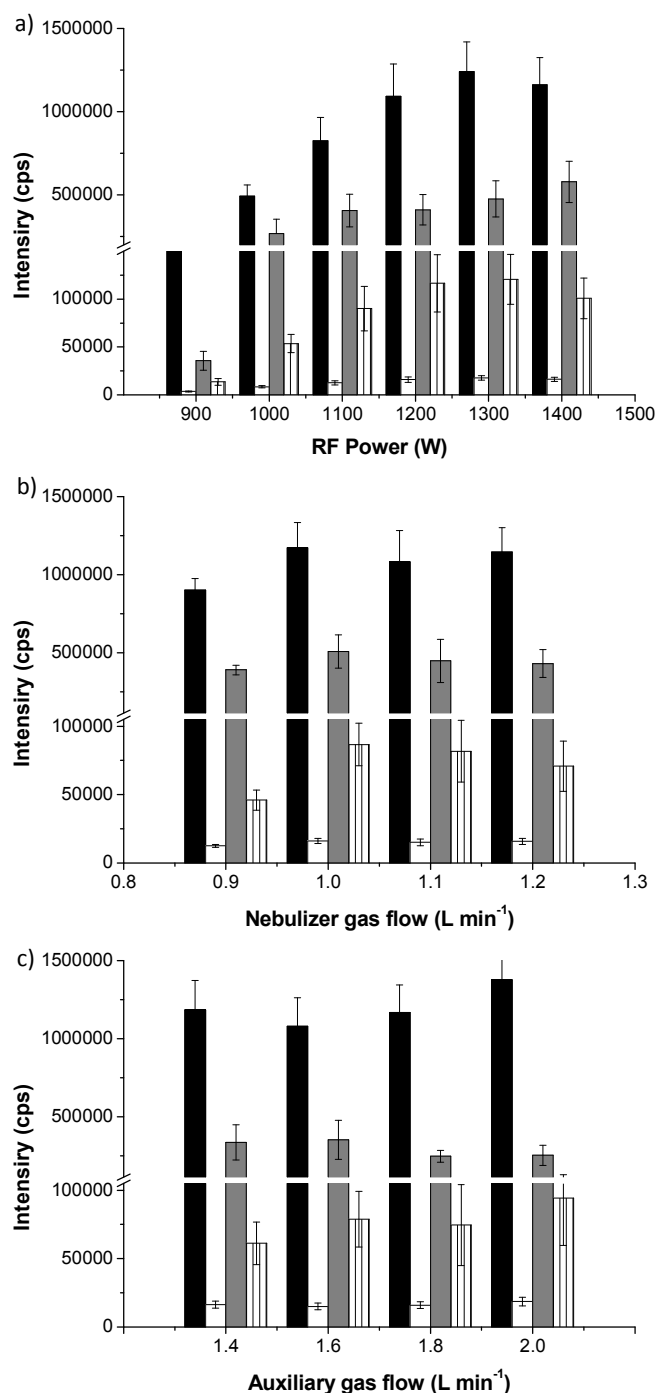


Figure 3 – Optimizations of ICP-MS parameters for image acquisition. Absolute intensities (cps) for $^{12}\text{C}^+$ (■), $^{13}\text{C}^+$ (□), $^{28}\text{Si}^+$ (■) and $^{31}\text{P}^+$ (▨), in relation to (a) RF power (W), (b) nebulizer gas flow rate (L min^{-1}) and (c) auxiliary gas flow rate (L min^{-1}).

since this element has a first ionization potential of $10.487 \text{ eV mol}^{-1}$. All the elements present a good signal to noise ratio for a RF power of 1300 W, and therefore this level was considered optimum for further experiments. It is interesting to comment that the RF power must be carefully controlled. This is because a high RF power can result in an excess of energy that promotes preferential ionization of other molecules (such as CO^+) or ions present in the matrix, resulting in a slight reduction of analytical signals, as observed in the Figure 3a for 1400 W RF.

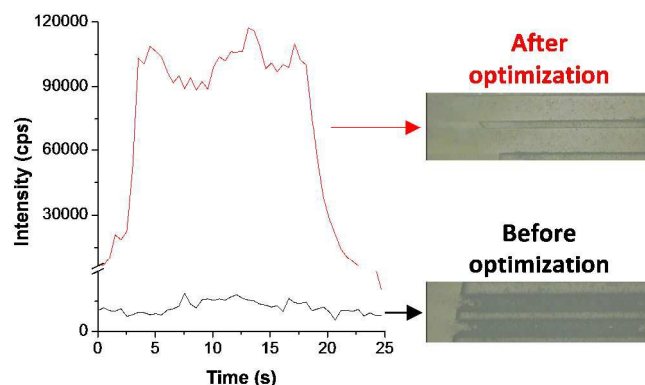


Figure 4 - Analytical signal for $^{31}\text{P}^+$ previous (–) and after the optimization (–).

The nebulizer gas carries the sample aerosol into the ICP and it is responsible for the plasma's toroid shape. Furthermore, it creates a channel through the center of the plasma, where the ion formation takes place.²⁹ Therefore the flow rates used as carrier gas were evaluated to optimize the transport of the ablated material and to obtain operational conditions for plasma stability. For this task, 0.9 to 1.2 L min^{-1} flow rates were evaluated. As noted in Figure 3b, a simple change in the nebulizer gas flow from 0.9 to 1.0 L min^{-1} was responsible for increasing the $^{31}\text{P}^+$ signal a 90%, highlighting the importance of this optimization. In fact, the highest signal was observed at 1.0 L min^{-1} for all elements monitored. At this level, the Ar used as a carrier gas can minimize the mass ablated deposition effect on the surface of the sample, thus improving the analyte transport to the ICP, and, as a consequence, the sensitivity.

The plasma geometry can also be influenced by the auxiliary gas flow rate. Then, this parameter was evaluated in a range comprised between 1.4 to 2.0 L min^{-1} . As shown in Figure 3c, this parameter did not influence the analytical signal, and for all monitored elements, the maximum gas flow rate available, 2.0 L min^{-1} , provided the highest signal. Further advantages of this flow rate are that (i) stability of the plasma is promoted, (ii) plasma extinction is avoided and (iii) ICP torch damages are greatly diminished.

A significant improvement was achieved in terms of ablation process when all the instrumental variables were settled in their optimum conditions. As shown in Figure 4, sample was partially removed by LA before optimization, but completely removed at the best-optimized conditions. This can be confirmed by the increase on the $^{31}\text{P}^+$ average signal from 1453 to 100000 cps (ca. 69 times). Additionally, the precision was improved as well, since RSD values decrease from 20.9 % to 7.3 %. At this point it was clear that, the proposed method was feasible for the evaluation of P distribution in tissue samples.

The internal standard method is usually used when the LA-ICP-MS is employed to address qualitative or quantitative studies, for overcoming the instrumental oscillations, which in turns can affect precision. Thus, the monitoring of one or more elements as internal standard is necessary as the normalization allows the differentiation between the natural occurrence of an analyte concentration in a specific point and its variability as a consequence of artifacts, such as local differences in tissue thickness or different interaction between the laser and the sample surface.^{17, 30-31}

Some conditions are needed for an element to be considered as internal standard, such as homogeneous distribution, constant concentration in the sample, and similar behavior to the analyte. Many strategies have been applied regarding the internal standard, e.g., the use of multiple standards or elements with low natural abundance. In this case, elements, such as ^{103}Rh or ^{185}Re , can be

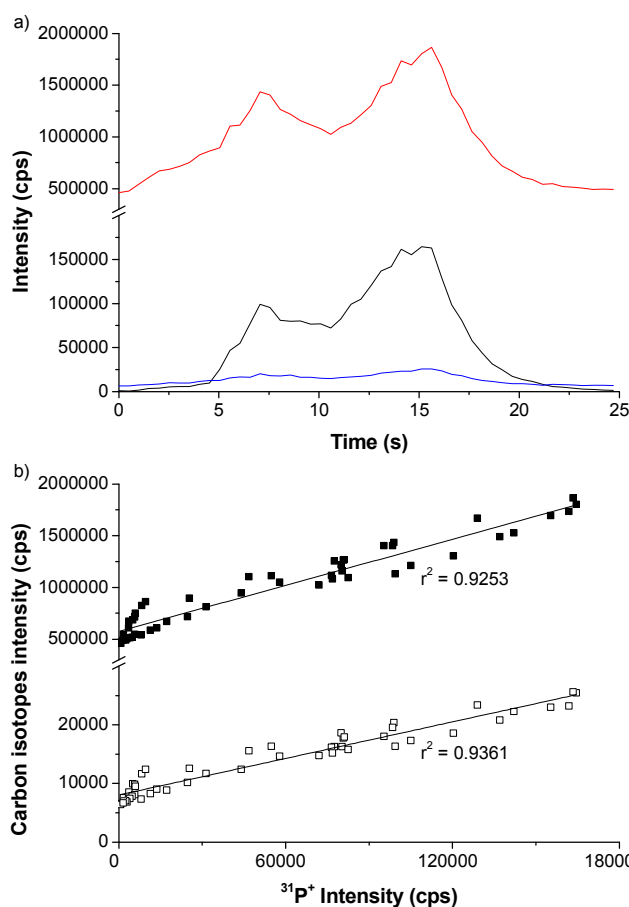


Figure 5 – Evaluation of carbon isotopes as internal standard. (a) Analytical signal for ions $^{12}\text{C}^+$ (—), $^{31}\text{P}^+$ (—) and $^{13}\text{C}^+$ (—) in tumor samples. (b) $^{31}\text{P}^+$ intensities in relation to $^{12}\text{C}^+$ (■) and $^{13}\text{C}^+$ (□).

monitored, or, alternatively a metal spiked polymer film (^{101}Ru or ^{89}Y).³⁰ However, in the majority of biological studies, the use of ^{12}C and ^{13}C has been the selected alternative, since these isotopes are the main components of tissues, and they match the above mentioned requisites in terms of homogeneity, concentration and behavior.^{17, 32}

In our case, ^{12}C and ^{13}C isotopes were monitored, presenting 21% and 16 % RSD values, respectively. Furthermore, a similar profile was obtained for carbon isotopes and $^{31}\text{P}^+$, as shown in Figure 5a. This can be confirmed by the comparison of the intensities between carbon isotopes and P^+ , since correlation coefficients of 0.9253 and 0.9361 for ^{12}C and ^{13}C , respectively were obtained, as shown in Figure 5b. Thus, both carbon isotopes can be considered as effective internal standards.

3.4. Building-up the image

A good synchronization between the laser speed and the ICP-MS acquisition rates is needed for a correct imaging analysis. In practical terms, data were collected by scanning the sample in different lines, employing the raster mode of the laser to generate the images. For ICP-MS (in this case a DRC-e, supplied by PerkinElmer), the acquisition of one line generates one file with format XBLite Program File (.xl extension), which provides a data sheet. In this file, the first column represents the acquisition time and the following columns show the results for all monitored analytes, while each row shows the results for each acquisition interval in the ICP-MS. It is important to note that other instruments from other manufacturers can provide data in several formats of file. However, the users have

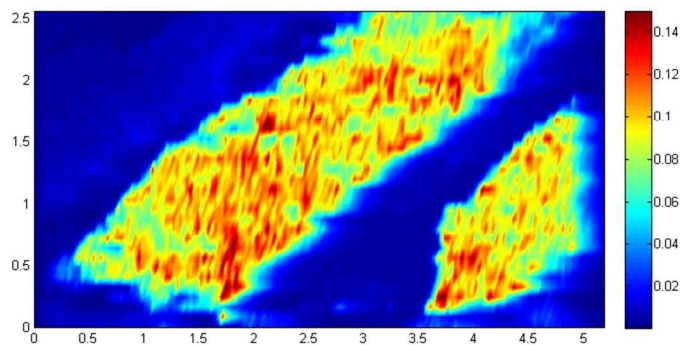


Figure 6 – Phosphorus distribution in penile cancer tumor sample. In this case, $^{12}\text{C}^+$ was used as internal standard.

only to save the data file in a compatible format to Excel for using this tutorial. Other softwares can be used to make images for LA-ICP-MS, such as Origin (Originlab Corporations, Northampton),³³ IMAGENA,³⁴ Pmod (Zurich, Switzerland),³⁵ the Python program ISIDAS in conjunction with Maya Vi2 (Enthought Inc.)³⁶ and SMAK-package.³⁷

During the ablation, the distance among the lines was 80 μm , providing the y-coordinate resolution for the two-dimensional image construction. Scan speed was 60 $\mu\text{m s}^{-1}$ in the LA system, and the acquisition time in the ICP-MS for each point was settled in 0.477 s. All LA-ICP-MS instrumental conditions are shown in Table 1.

For a better comprehension of our strategy, all steps regarding data treatment are properly addressed in the supplementary material (SM) section. The acquisition of two-dimensional images was performed in accordance to the method proposed by Silva & Arruda.⁹ Thus, the files obtained from the ICP-MS acquisition (XBLite Program File) were exported as Microsoft Excel (please refers to slides 1-8 SM) files. Each line generated through the ablation process was exported to different worksheet in the Excel (see slide 7 – SM). Thus, if the sample ablation requires 50 lines for mapping the entire sample surface, then 50 XBLite files will be generated, and each one will be exported to a unique sheet, totaling 50 Excel worksheets. It is important to mind that each worksheet contains the results of all analytes selected for monitoring the elemental distribution in the sample (see slide 9 – SM). Thus, the next step is to organize the results of each element in a single worksheet. This task can be accomplished using the commands "copy" and "paste". In this step, the results of one element must be copied from the original worksheet, and then, pasted into a new worksheet, following the sequence of the ablation process and signal acquisition (see the slides from 13 to 16 – SM). Through this process, the treatment of the results is easier to perform. Blanks are made by acquired data from the argon atmosphere without any ablation process (see slides from 17 to 20), and their signals subtracted from sample signals. The normalization of results was also carried out using an internal standard (see slides from 21 to 22). Finally, all the excel files were converted into a text file (tab delimited, file format .txt) to make easier the construction of the image using MATLAB (see slides from 24 to 27 – SM).

In this software, results made up a matrix data, which was responsible for providing the analyte distribution in the sample (see slide 26 – SM). A MATLAB routine was used for the building of two-dimensional images. This 2D-image was created by a plan with coordinates (x, y), where x was obtained from the number of points collected by ICP-MS and y was based on the number of lines used to generate an image. It is crucial to note that there was a z value for each coordinate. Thus, the matrix plane (x, y) was correlated with the

data matrix z (intensity for each point), providing the image with the analyte distribution in the sample.

For x -axis definition, the ICP-MS acquisition time was considered, as well as the LA system scan speed. Regarding these parameters, the data sets were separated by intervals of 31.62 μm , thus obtaining an x -axis total size of 5.19 mm (see slide 34 – SM). Concerning y -axis, it was just defined by the spacing among the lines, which, in our case, was 80 μm , and a y -axis total size of 2.56 mm was then obtained (see slide 35 – SM). Data were converted into a matrix plane (x, y) through the command “[x,y]=meshgrid(x,y)”, in the MATLAB (see slide 36 – SM).

In the case of data acquisition in the horizontal position (laser position in the horizontal profile), a transpose function ($w=z'$) is necessary to adjust the image, once that data are storage in the program as columns (vertical position). Then, this function rotates all data, maintaining the relative intensity of each point (see slide 37 – SM).

The image was then obtained by the command “pcolor (x,y,z)” or “pcolor (x,y,w)” depending on the position of acquisition data in LA system, as previously described (see slide 38 and 39 – SM). All treatments concerning on the image smoothing, colormap definition and colorbar insertion can be visualized from slide 40 to 51 in the SM. For imaging edition, the operator needs to click in Edit, and then Figure properties (see slide 40 – SM).

By clicking on the figure (see slide 41 – SM), the software option was selected, and after chosen Edges flap, the option “no line” was selected (slide 42 – SM).

Regarding image smoothing, two different tools are available in the MATLAB, which were used in a sequence, in order to improve image resolution. The first one was that using the Faces flap, and chosen “blended” (see slide 43 – SM). By clicking in More properties (see slide 44), following the sequence: lighting – facelighting – phong (slide 45 – SM), which the final result is visualized in the slide 46 – SM.

The Colormap (slide 47) is related to the intensity of the image, and it can be edited by clicking the sequence (1) Edit and then (2) color map. Then, Color map editor flap appears (slide 48), giving the possibility to set the minimum and maximum color data levels (in our case, 0.0004 and 0.15, respectively). The final figure can present the Colorbar, which shelters the interval data defined in the Colormap. For this task, goes to command window and click in Insert and then in Colorbar (see slide 49 – SM). MATLAB software allows data storage in several file formats compatible with different platforms for text edition. In our case, the image was saved as a Tagged Image File Format (or TIFF) image (see slide 51 – SM).

The definition of some parameters, such as blended, facelighting, phong, among others, can be found in the tutorial of the MATLAB program. The image of penile cancer sample is shown in Figure 6.

Finally, it is worth to mention that in this work images were obtained for the qualitative elemental distribution in a tissue, for example, once that for establishing the actual concentration of each element and at each image point, it would be necessary data validation, which was not covered in this work.

4. Conclusions

The objective of this tutorial was to provide the analytical basis for handling LA-ICP-MS imaging technique. The main instrumental parameters involving both, laser and ICP were evaluated and properly discussed, thus producing a guide for experts and non-experts that helps the analyst in the acquisition of reliable data. The laser parameters that greatly influence the results are (i) ablation intensity, (ii) frequency and (iii) spot size. Considering the ICP-MS those parameters that mostly influence the results were (i)

radiofrequency, (ii) flow rate gases (auxiliary and nebulizer) and (iii) internal standards.

After optimizing all the above mentioned parameters, those necessary steps for building-up the images, such as (i) data acquisition, (ii) data exporting, (iii) data treatment, and those involved in the creation of the two-dimensional image, through the MATLAB program have been explained also.

Finally, this practical guide makes easier the work with LA-ICP-MS, opening the window for creating in-house methods for imaging any kind of tissue.

Acknowledgements

The authors thank the Fundação de Amparo a Pesquisa do Estado de São Paulo (FAPESP, São Paulo, Brazil), the Conselho Nacional de Desenvolvimento Científico e Tecnológico (CNPq, Brasília, Brazil), and Cordenadoria de Aperfeiçoamento de Pessoal de Nível Superior (CAPES, Brasília, Brazil) for financial support. The authors are also thank to Prof. Sílvia R. Rogatto for providing the sample material. H. López-Fernández was supported by a pre-doctoral fellowship from Xunta de Galicia.

Notes and references

^a Group of Spectrometry, Sample Preparation and Mechanization (GEPAM), Institute of Chemistry, PO Box 6154, University of Campinas, UNICAMP, 13084-862, Campinas, SP, Brazil

* E-mail: zezzi@iqm.unicamp.br

^b National Institute of Science and Technology for Bioanalytics, Institute of Chemistry, University of Campinas, UNICAMP, 13084-862, Campinas, SP, Brazil

^c UCIBIO-REQUIMTE, Chemistry Department, Faculty of Science and Technology, University NOVA of Lisbon, 2829-516, Monte da Caparica, Portugal

^d ProteoMass Scientific Society, Madan Parque, Rua dos Inventores, 2825-182, Caparica, Portugal.

^e Escuela Superior de Ingeniería Informática, Edificio Politécnico, Campus Universitario As Lagoas s/n, University of Vigo, 32004 Ourense, Spain

^f CITI: Centro de Investigación, Transferencia e Innovación, Parque Tecnológico de Galicia – Tecnópole, Avda. de Galicia N 2, San Ciprián das Viñas, 32900 Ourense, Spain

- 1 A. Brisbane, *Syracuse Post Standard*, 1911, **28**, 18.
- 2 J. Rimola, A. Forner, S. Tremosini, M. Reig, R. Vilana, L. Bianchi, C. Rodríguez-Lopes, M. Solé, C. Ayuso and J. Bruix, *J. Hepatol.*, 2012, **56**, 1317.
- 3 J. J. Muñoz, S. A. Drigo, M. C. Barros-Filho, F. A. Marchi, C. Scapulatempo-Neto, G. S. Pessoa, G. C. Guimaraes, J. C. S. Trindade Filho, A. Lopes, M. A. Z. Arruda and S. R. R. Rogatto, *J. Urol.*, 2014, **194**, 245.
- 4 E. H. Seeley and R. M. Caprioli, *Trends in Biotechnol.*, 2011, **29**, 136.
- 5 N. Braidly, A. Poljak, C. Marjo, H. Rutledge, A. Rich, T. Jayasena, N. C. Inestrosa and P. Sachdev, *Front. Aging Neurosci.*, 2014, **6**, 138.
- 6 J. Yao, M. Yang and Y. Duan, *Chem. Rev.*, 2014, **114**, 6130.
- 7 J. S. Becker, M. V. Zoriy, C. Pickhardt, N. Palomero-Gallagher and K. Zilles, *Anal. Chem.*, 2005, **77**, 3208.
- 8 B. C. M. Maciel, H. S. Barbosa, G. S. Pessoa, M. M. Salazar, G. A. G. Pereira, D. C. Gonçalves, C. H. I. Ramos and M. A. Z. Arruda, *Proteomics*, 2014, **14**, 904.
- 9 M. A. O. Silva and M. A. Z.; Arruda, *Metallomics*, 2013, **5**, 62.
- 10 S. R. Oliveira and M. A. Z. Arruda, *J. Anal. At. Spectrom.* 2015, **30**, 389.

- 1
2
3
4
5
6
7
8
9
10
11
12
13
14
15
16
17
18
19
20
21
22
23
24
25
26
27
28
29
30
31
32
33
34
35
36
37
38
39
40
41
42
43
44
45
46
47
48
49
50
51
52
53
54
55
56
57
58
59
60
- 11 I. Lavilla, M. Costas, P. San Miguel, J. Millos, C. Bendicho, *Biometals*, 2009, **22**, 863.
 - 12 V. R. Bhatt, R. G. Bociek, J. Yuan, K. Fu, T. C. Greiner, B. J. Dave, S. K. Rajan, and J. O. Armitage, *J. Natl. Compr. Cancer Network*, 2015, **13**, 281.
 - 13 H. Wang, B. Wang, M. Wang, L. Zheng, H. Chen, Z. Chai, Y. Zhao and W. Feng, *Analyst*, 2015, **140**, 523.
 - 14 J. N. Eble, G. Sauter, J. I. Epstein, and I. A. Sesterhenn, *WHO Classification of Tumors: Pathology and Genetics of Tumours of the Urinary System and Male Genital Organs*. IARC Press, Lyon, **2004**, 359p.
 - 15 V. Trunova, A. Sidorina, V. Zvereva, and B. Churin, *J. Trace Elem. Med. Biol.*, 2013, **27**, 76.
 - 16 H. Boonstra, J. W. Oosterhuis, A. M. Oosterhuis, and G. J. Fleuren, *Virchows Arch A Pathol Anat Histopathol.*, 1983, **402**, 195.
 - 17 J. Sabine Becker, A. Matusch, and B. Wu, *Anal. Chim Acta.*, 2014, **835**, 1.
 - 18 D. Hare, C. Austin, and P. Doble, *Analyst*, 2012, **137**, 1527.
 - 19 S. F. Durrant, and N. I. Ward, *J. Anal. At. Spectrom.*, 2005, **20**, 821.
 - 20 K. Jurowski, M. Szewczyk, W. Piekoszewski, M. Herman, B. Szewczyk, G. Nowak, S. Walas, N. Miliszkievicz, A. Tobiasz, and J. Dobrowolska-Iwanek, *J. Anal. At. Spectrom.*, 2014, **29**, 1425.
 - 21 V. L. Dressler, D. Pozebon, M. F. Mesko, A. Matusch, U. Kumtaptim, B. Wu, and J. Sabine Becker, *Talanta*, 2010, **82**, 1770.
 - 22 S. F. Boulyga, C. Pickhardt, and J. S. Becker, *At. Spectrosc.*, 2004, **25**, 53.
 - 23 D. Gunther, S. E. Jackson, and H. P. Longrich, *Spectrochim. Acta, Part B*, 1999, **54**, 381.
 - 24 M. R. Florez, M. Aramendia, M. Resano, A. C. Lapena, L. Balcaen, and F. Vanhaecke, *J. Anal. At. Spectrom.*, 2013, **28**, 1005.
 - 25 D. S. Urgast and J. Feldmann, *J. Anal. At. Spectrom.*, 2013, **28**, 1367.
 - 26 D. S. Urgast, S. Hill, I. S. Kwun, J. H. Beattie, H. Goenaga-Infante, and J. Feldmann, *Metallomics*, 2012, **4**, 1057.
 - 27 J. Feldmann, A. Kindness and P. Ek, *J. Anal. At. Spectrom.*, 2002, **17**, 813.
 - 28 R. Thomas, *Practical guide to ICP-MS: a tutorial for beginners*. 2nd ed. CRC Press, Boca Raton, **2008**, 324p.
 - 29 F. Vanhaecke and P. Degryse, *Isotopic Analysis: fundamentals and applications using ICP-MS*. Wiley-VCH, Weinheim, **2012**, 529p.
 - 30 K. Jurowski, B. Buszewski and W. Piekoszewski, *Talanta*, 2015, **131**, 273.
 - 31 K. Jurowski, S. Walas and W. Piekoszewski, *Talanta*, 2013, **115**, 195.
 - 32 D. A. Frick and D. Günther, *J. Anal. At. Spectrom.*, 2012, **27**, 1294.
 - 33 P. Nemes, A. A. Barton, Y. Li, and A. Vertes, *Anal. Chem.*, 2008, **80**, 4575.
 - 34 T. Osterholt, D. Salber, A. Matusch, J.S. Becker, and C. Palm, *Int. J. Mass Spectrom.*, 2011, **307**, 232.
 - 35 A. Matusch, L. S. Fenn, C. Depboylu, M. Kliez, S. Strohmer, J. A. McLean, and J. S. Becker, *Anal. Chem.*, 2012, **84**, 3170.
 - 36 C. Austin, T. M. Smith, A. Bradman, K. Hinde, R. Joannes-Boyau, D. Bishop, D. J. Hare, P. Doble, B. Eskenazi, and M. Arora, *Nature.*, 2013, **498**, 216.
 - 37 B. P. Jackson, D. Bugge, J. F. Ranville, and C. Y. Chen, *Environ Sci. Technol.*, 2012, **46**, 5550.